Efficient and high-resolution simulation of pollutant dispersion in complex urban environments by island-based recurrence CFD

Environmental Modelling and Software 145 (2021) 105172

Contents lists available at ScienceDirect

Environmental Modelling and Software

journal homepage: www.elsevier.com/locate/envsoft

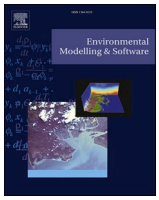

Efficient and high-resolution simulation of pollutant dispersion in complex urban environments by island-based recurrence CFD

Yaxing Du [a], Bert Blocken [b,c], Sanaz Abbasi [a], Stefan Pirker [a,*]

[a] Department of Particulate Flow Modelling, Johannes Kepler University, Linz, Austria
[b] Building Physics and Services, Department of the Built Environment, Eindhoven University of Technology, Eindhoven, Netherlands
[c] Building Physics and Sustainable Design, Department of Civil Engineering, KU Leuven, Leuven, Belgium

ARTICLE INFO

Keywords:
Recurrence CFD (rCFD)
Pollutant dispersion
Island-based rCFD
Real-time CFD

ABSTRACT

We applied data-based recurrence CFD (rCFD) to model pollutant dispersion in near-field flow configurations. In case of complex topologies, the global-domain version of rCFD fails to account for local recurrent flow features. We therefore developed a novel island-based version of rCFD, which partitions the computational domain to isolate islands of high recurrence prominence, and subsequently defines a distinct recurrence path for each of these islands. We applied island-based rCFD to pollutant dispersion for two side-by-side cubical buildings with three different gap widths in between them and a real urban environment. We showed that numerical predictions of pollutant dispersion by island-based rCFD were in excellent agreement with full CFD simulations, thus outperforming the global-domain version of rCFD. In both applications, island-based rCFD simulations ran three orders of magnitude faster than corresponding full CFD simulations. In the second application, this speed-up enabled real-time simulations on a computational grid of 10 million cells.

1. Introduction

Globally, over 50% of the population lives in urban areas today, and the world's urban population will increase to 7.5 billion before 2050 (Giles-Corti et al., 2016). In recent years, air pollution in urban environments has increased significantly, posing a serious societal problem (Environmental Protection Agency, 2020; Zhong et al., 2016). Air quality in compact urban environments is directly linked to human health (Block and Calderón-Garcidueñas, 2009; Shorshani et al., 2015) because of daily exposure to hazardous pollutants by outdoor activities and the penetration of outdoor pollutants into the indoor environment by building ventilation and infiltration. The urban outdoor air pollution originates mainly from emissions from traffic, households and industry and comprises hazardous materials (e.g., toxic gaseous substances and fine particulates) (Bartzis et al., 2008; Shorshani et al., 2015). Understanding pollutant dispersion mechanisms and identifying pollution concentration patterns is essential for the design of pollution mitigation strategies.

For the investigation of pollutant dispersion in urban environments different approaches, like field measurements (Cui et al., 2017; Niu and Tung, 2007), wind tunnel tests (Gromke et al., 2016; Gromke and Ruck, 2012), and numerical simulations (Blocken, 2014; Blocken and Gualtieri, 2012; Tominaga and Stathopoulos, 2013) have been employed. Especially, numerical simulations have been widely used because of their relatively low cost and for their ability to provide three-dimensional information in the whole computational domain, as opposed to point measurements in field measurements and wind tunnel tests.

Among numerical simulations and analytical calculations, Gaussian dispersion models are often utilized because of their simplicity and time efficiency (Moonen and Allegrini, 2015; Rajaona et al., 2015; Senocak et al., 2008). However, these simple models fail to capture near-field dispersion mechanisms and three-dimensional concentration patterns within complex urban topologies. In such cases, computational fluid dynamics (CFD) simulations have been proposed to accurately simulate the interaction between the complex wind field and the pollutant (Blocken et al., 2013; Chu et al., 2005; Gousseau et al., 2012).

On top of the complex mean flow, pollutant dispersion is governed by the turbulence characteristics (i.e. the characteristics of the large-scale and small-scale vortices) of the flow. In the context of CFD simulation of urban flows, especially these small-scale flow features cannot be resolved but their effect on the mean flow has to be modelled by an appropriate turbulence model. Generally, turbulence models can be roughly organized into Reyonds-averaged Navier-Stokes (RANS) models

* Corresponding author.
E-mail address: stefan.pirker@jku.at (S. Pirker).

https://doi.org/10.1016/j.envsoft.2021.105172
Accepted 18 August 2021
Available online 2 September 2021

and Large Eddy Simulation (LES) models.

RANS models are based on time-averaging of turbulent fluctuations (independent of their spatial scale) and require less computational resources than LES. Consequently, they have been utilized in many urban environmental studies, (e.g. Ai and Mak, 2014; Blocken et al., 2012; Du et al., 2018; Ricci et al., 2019). LES models, in turn, resolve large-scale turbulent fluctuations, while only the spatially small scales are modelled by a sub-grid model (Pope, 2000). Recently, LES models have been used in studies of near-field pollutant dispersion in built-up environments (Blocken, 2018; Moonen et al., 2011), indicating a higher predictive capability of LES over RANS models.

The large drawback of LES turbulence models is the associated computational cost which is much higher than that of RANS models. Tominaga and Stathopoulos (2013) reported that the computational time of LES was 10–25 times higher than that of a comparable RANS simulation. Therefore, increasing the computational efficiency of LES without significant loss in accuracy can be seen as a major requirement and challenge towards a wider spread application of LES in near-field pollutant dispersion modeling.

For the case of pseudo-periodic flows (which can be described by recurring flow features), the recurrence CFD (rCFD) approach was developed to mitigate the high computational costs of LES. Recurrence CFD was first developed in the realm of chemical engineering (Lichtenegger and Pirker, 2016; Pirker and Lichtenegger, 2018), and has been successfully applied in several fields, including bubble columns (Abbasi et al., 2020), fluidized beds (Dabbagh et al., 2020), and free surface flows (Pirker et al., 2020). Conceptually, rCFD is a data-assisted method, employing a two-stage strategy of data storage and data utilization. In the first stage, conventional CFD simulations are utilized to generate a characteristic database representing the flow field under consideration; and in the second stage, this database is exploited to picture the propagation of passive scalars (like an air pollutant). Following this simple strategy, the computational times of scalar dispersion processes have been significantly reduced, resulting in a speed-up of three to four orders of magnitude by rCFD in comparison to full CFD simulations (Dabbagh et al., 2020; Du et al., 2020; Pirker and Lichtenegger, 2018; Pirker et al., 2020).

In our previous work, we successfully applied rCFD to accurately predict pollutant dispersion around an isolated cubical building benchmark case (Du et al., 2020). In that study, we could reduce the computational time of corresponding LES-based CFD simulations by three orders of magnitude without impairing neither the resolution nor the accuracy of results. However, the step from this benchmark case towards complex flows in urban topologies is not straightforward. At its core, the rCFD method relies on a prominent recurrent nature of the flow, such that within the database (which is provided a priori by conventional CFD simulations) one always finds pairings of similar flow patterns at two instances of time. While this was possible for the simple benchmark case, it might be impossible for more complex topologies. In his study on local and global recurrence, Lichtenegger (2018) showed that the global dimensionality of a flow scales exponentially with the domain size. In order to meet this dimensionality, we would have to build up huge databases spanning a very long observation period before we can find a pair of globally similar flow patterns. At first glance, this restriction might render the application of rCFD to complex flows in large domains impossible.

In this study, we try to overcome this existing limitation of rCFD by a domain decomposition approach such that we organize the global domain into smaller recurrence islands, which for themselves are appropriate for an application of rCFD. For this purpose, we first have to identify sub-domains of prominent recurrent flow features (such as wakes of buildings), which are embedded in a background flow of low prominence (in our case, prominent recurrent flow features manifest in a large magnitude of local vorticity fluctuations, see Section 2.2). Once identified, the databases for those recurrence islands are built up, which are then exploited for the simulation of local dispersion. On a deeper code level, these local recurrence islands required a thorough revision and adaption of the existing cell-to-cell shift operator in rCFD, which represents convective fluxes. In order to test this island-based rCFD approach, we first illustrate its functionality for the case of two side-by-side cubic buildings with a gap of varying width between them (the configuration of cubical building and the incident wind profile are adopted from the experimental setup of Li and Meroney (1983)). While in case of a small gap, separating the wakes into independent recurrence islands does not make sense, because of the dominant wake interactions, it does become a viable option for larger gap widths. In this purely numerical study, we will study pollutant dispersion from a ground-level line source in the wake of the two buildings by comparing the predictions of full LES-based CFD, existing global-domain rCFD and our novel island-based rCFD. In a second part of this study, we apply island-based rCFD to the complex urban topology of the Wissensturm neighborhood in the City of Linz, Austria. Also in this case, a ground level line source emission is considered, which represents vehicular exhaust along a street, and we critically compare the predictions of full LES-based CFD and island-based rCFD.

This paper is structured as follows: In Section 2, the methodologies of full LES-based CFD, the existing rCFD and the novel island-based rCFD are presented. Afterwards, predictions of pollutant dispersion are presented and analyzed for the side-by-side cubical buildings in Section 3, and for the real urban environment in Section 4, respectively. Finally, summary and conclusions are given in Section 5.

2. Method

2.1. Conventional LES-based CFD simulations

In the framework of this study, conventional LES-based CFD simulations are run for two purposes. On the one hand, short-term full CFD simulations are used to feed the database for subsequent rCFD simulations, while on the other hand, long-term full CFD simulation serve as numerical validation base for our novel rCFD method.

Since the LES-based CFD simulation methodology has been presented in our previous publication (Du et al., 2020), we omit any details in the present paper. In the following, we only briefly rephrase the main concept for the sake of completeness.

The governing filtered Navier-Stokes equations for incompressible, isothermal fluid flow of a Newtonian fluid read

$$\frac{\partial \overline{u}_i}{\partial x_i} = 0, \tag{1}$$

and

$$\frac{\partial \overline{u}_i}{\partial t} + \frac{\partial\left(\overline{u}_i \overline{u}_j\right)}{\partial x_j} = \upsilon \frac{\partial^2 \overline{u}_i}{\partial x_j x_j} - \frac{1}{\rho}\frac{\partial \overline{p}}{\partial x_i} - \frac{\partial \tau_{ij}}{\partial x_j}. \tag{2}$$

where u_i is the Cartesian velocity component, p represents the pressure (the overbars indicate spatial filtering) and υ is the molecular viscosity. The subgrid-scale stress tensor, τ_{ij}, describes the effect of unresolved turbulent eddies and can be modelled as (Pope., 2000),

$$\tau_{ij} - \frac{1}{3}\tau_{kk}\delta_{ij} = -2\mu_t \overline{S}_{ij}, \tag{3}$$

with, τ_{kk} being the isotropic part of subgrid-scale stress, $\overline{S}_{ij}$ representing the rate-of-strain tensor for the resolved scale and μ_t denotes the subgrid-scale turbulent viscosity. In the Smagorinsky–Lilly subgrid-scale model (Lilly, 1966; Smagorinsky, 1963), μ_t is modelled by (Fluent., 2018)

$$\mu_t = \rho L_s^2 \left|\overline{S}\right|, \tag{4}$$

with $\left|\overline{S}\right| \equiv \sqrt{2\overline{S}_{ij}\overline{S}_{ij}}$ and L_s the mixing length which, in turn, is calculated

by,

$$L_s = min\left(kd, C_s V^{1/3}\right) \tag{5}$$

where $k = 0.40$ is the von Kármán constant, d is the closest wall distance, V is the volume of the computational cell and $C_s = 0.1$ is the Smagorinsky constant.

On top of the flow equations, the transport equation for the passive scalar φ (e.g. a pollutant concentration) reads,

$$\frac{\partial \overline{\varphi}}{\partial t} + \frac{\partial\left(\overline{\varphi u_i}\right)}{\partial x_i} = -\frac{\partial}{\partial x_i} D_{eff} \frac{\partial \overline{\varphi}}{\partial x_i} + \overline{s}, \tag{6}$$

with D_{eff} as the effective diffusivity and $\overline{s}$ representing a source term (e.g. a pollution source).

2.2. Existing recurrence CFD simulations

As with the conventional LES-based simulations, the existing recurrence CFD (rCFD) approach has been presented in detail in our previous publication (Du et al., 2020). In the present paper, we therefore restrict ourselves to restating the main concept of rCFD. However, in presenting the main ingredients of rCFD, we will emphasise the description of the recurrent nature of the flow (more specifically, the recurrence prominence), since this will pave the way for the novel island-based version of rCFD.

As stated in the introduction, rCFD is a data-assisted approach employing a two-phase strategy. First, a characteristic database of the given pseudo-periodic flow is generated using conventional LES-based CFD simulations. In this phase, the fluid flow is traced by massless particles, and in regular intervals start and end positions of those Lagrangian tracer paths are stored as characteristic cell-to-cell communication paths into a database (which, in the end, consists of N frames of cell-to-cell communication patterns). In a second phase, this database is utilized by a Markov-alike recurrence process which stitches together sequences from the database. More specifically, this results into a cell-to-cell communication network, which can evolve beyond the time-span of the characteristic database. Based on this recurrent communication network, any passive scalars can be transported according to the pre-set cell-to-cell communication paths. In our previous work (Du et al., 2020), we additionally revised the face-swap operator, which accounts for the physical diffusion of air pollutants.

In order to describe the degree of similarity between two frames in the database (describing two flow fields at two instances of time, t and t'), we employ a recurrence norm,

$$N_{rec}(t,t') \equiv \frac{\int d^3r(\phi(\boldsymbol{r},t) - \phi(\boldsymbol{r},t'))^2}{max_{t,t'} \int d^3r(\phi(\boldsymbol{r},t) - \phi(\boldsymbol{r},t'))^2}, \tag{7}$$

with $\boldsymbol{r}$ as spatial coordinate and the integral represents integration over the whole domain. In order to capture the recurrent nature of a given flow most efficiently, the field quantity ϕ should be chosen based on the physical core phenomenon under consideration. In our case, we opted for the fluctuating component of the flow vorticity, $\phi = \widetilde{\boldsymbol{\omega}} = |\boldsymbol{\omega} - \langle \boldsymbol{\omega} \rangle|$, with $\boldsymbol{\omega} = \nabla \times \boldsymbol{u}$ and $\langle \cdot \rangle$ indicating time averaging.

Once the pairwise recurrence norms have been calculated, we can span a recurrence matrix which indicates the degree of similarity between frame pairings within the database (see illustration in Fig. 1). Obviously, this recurrence matrix has a zero diagonal since the recurrence norm between identical frames is zero. In the off-diagonal region, however, the value of the recurrence norm first increases (i.e. the level of similarity between frames decreases) before it eventually starts to fluctuate around a rather constant value, the recurrence plateau. If the off-diagonal values of the recurrence norm do not run into a plateau, the observation period for the database, τ_{rec}, was too small or the flow cannot be considered as pseudo-periodic. If we just plot the recurrence norm along the first line of the recurrence matrix, we obtain a recurrence vector, which clearly illustrates this off-diagonal behaviour of the recurrence norm (Fig. 1, right). Starting from zero, the recurrence norm first increases, before it fluctuates around the recurrence plateau. Finally, the magnitude of these fluctuations represents the prominence of recurrence. Essentially, this recurrence prominence determines how well we can distinguish between similar and non-similar frame pairings within the database.

While in our previous study on the isolated cube benchmark case (Du et al., 2020), we experienced significant recurrence prominence of this local flow configuration, we obtain a very low recurrence prominence for the case of large domains of complex topologies (shown later in this study).

2.3. Novel island-based recurrence CFD simulations

At its core, our novel island-based recurrence CFD methodology introduces a spatial domain composition depending on the local

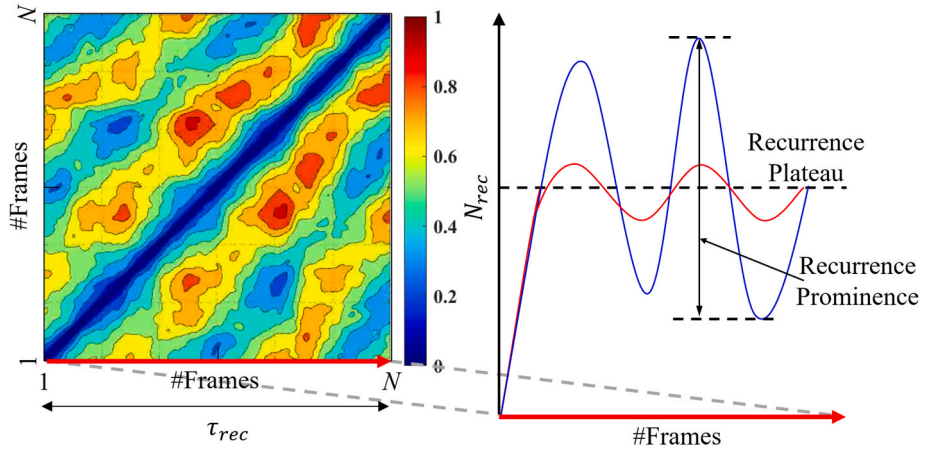

Fig. 1. Sketch of (left) a typical recurrence matrix (of arbitrary values) with the red arrow indicating the position of the recurrence vector and (right) a recurrence vector picturing two typical off-diagonal recurrent norm functions (of arbitrary values) for recurrent flows with (blue) high and (red) low recurrence prominence.

prominence of recurrent flow features. In the following sub-section, we will introduce this island identification methodology, while further implications of this domain decomposition are addressed in subsection 2.3.2.

2.3.1. Identification of recurrence islands

For the identification of recurrence islands, we use the same field quantity as we have proposed for the recurrence norm (Eq. (7)). Hence, we try to identify local regions (islands) of high fluctuations of vorticity, $\widetilde{\omega}$. The main steps of this identification procedure are sketched in Fig. 2 and can be summarized as follows. First, the time-averaged field of vorticity fluctuations $\widetilde{\omega}$ is spatially smoothened in order to avoid excessively small islands. Second, we look for remaining local maxima and starting from those maxima, we expand individual islands towards their neighbouring cells until another island is reached. Typically, this procedure results in quite a lot of small and maybe neighbouring recurrence islands. Therefore, closely located small islands are combined into larger ones in a third step in order to achieve a reasonable number of individual recurrence islands.

2.3.2. Island-based rCFD approach

Once recurrence islands are identified, we can build a recurrence matrix for each of those sub-domains. Consequently, we will find different recurrence paths which result in individual time-varying communication networks (of cell-to-cell shift patterns) for each island. In Fig. 3 the main consequence for the existing recurrence CFD is emphasized. Instead of one global-domain communication network, we have N networks, which are controled by different recurrence paths. During the convection step, we have to loop through individual sets of cell-to-cell shifts for each recurrence island. Notably, all other steps of the recurrence CFD algorithm remain unaffected by this domain decomposition.

2.4. Numerical implementation

The novel island-based rCFD runs on the same computational grid as the conventional CFD simulation. Furthermore, all functionalities of the island-based rCFD approach have been implemented in the framework of ANSYS Fluent V19.2 by User Defined Functions such that there is no need to switch the software between full CFD and rCFD simulations. However, the fluid solver functionalities of Fluent will only be used for feeding the database. The rCFD solver only uses Fluent's grid access routines (i.e. cell to face pointers), parallel communication (by MPI-macros) and post-processing functions.

3. Application 1: two side-by-side cubical buildings

In order to prove the functionality of our novel island-based rCFD approach, we consider the example of two side-by-side cubical buildings with a gap in between. In the next three sub-sections, we start with a description of the case set-up as well as the numerical settings for both conventional LES-based CFD simulations and rCFD simulations, respectively. Finally, subsection 3.4 is dedicated to a thorough analysis of the predictions of the existing global-domain rCFD and our novel island-based rCFD in comparison to reference results of long-term full conventional CFD simulations.

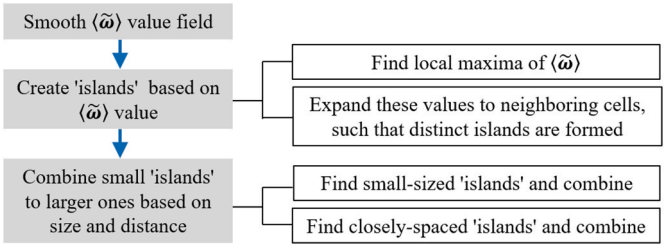

Fig. 2. Three-step process of the recurrence island identification.

3.1. Case setup

We adopt the case setup from the wind tunnel experiments of Li and Meroney (1983) who studied pollutant dispersion from a vent on the roof of a cubical building. In our previous work (Du et al., 2020), we validated conventional LES-based CFD simulations for this specific setup, and performed sensitivity tests of spatial and temporal discretization. In this study, we essentially used the same cube geometry, boundary conditions and temporal discretization and similar spatial discretization as in the previous work, but we doubled the cubic building to arrange for the side-by-side configuration of two buildings with a gap. In total, we consider three side-by-side configurations by changing the gap width between the two cubical buildings from one to five times of building height, as detailed in Fig. 4. These three configurations are called Gap-1, Gap-3 and Gap-5, respectively.

To represent the vehicular exhausts in the street, a ground-level line source downstream of the two side-by-side buildings is defined. The line source is placed 0.025 m downstream of the buildings and stretches along both buildings such that the line length is equal to two time the building length plus the gap width (see Fig. 5). Vehicular exhausts are simulated by means of a passive tracer gas with same density as air and the emission rate is set to 3.0×10^{-5} kg/s.

3.2. Simulation settings for conventional CFD

The size of the computational domain was chosen in alignment with best practice guidelines (BPGs) (Schatzmann et al., 2010; Tominaga et al., 2008), resulting in dimensions of 21H (length) × (12H + G) (width) × 6H (height), based on the building height H (Fig. 5a). The grid topology and numerical settings are directly adopted from our previous work (Du et al., 2020). At the building surfaces, the distance of first cell center-point to the wall is set to 0.00125 m, yielding y* values of about one. The computational grid for the three gap widths consists of 1.4, 1.7 and 2.1 million hexahedral cells (Fig. 5b). The vertical inlet wind profile as well as the profiles for turbulent energy and turbulent dissipation rate are deduced from the experiment of Li and Meroney (1983). The SIMPLEC algorithm is applied for pressure-velocity coupling and second-order schemes are used for temporal and spatial derivatives. Further details are given in our previous publication (Du et al., 2020).

After an initial spin-up process, a pseudo-periodic flow is established after roughly two flow-through times, with the latter being defined as $\tau_f = L/U_H = 0.32\,s$, with $L = 1.05$ m the length of computational domain and U_H as = 3.3 m/s the characteristic wind profile velocity at building height. After these two flow-through times, the data sampling for the rCFD database starts, while at the same time, a long-term (40 x τ_f) LES-based CFD simulation of pollutant dispersion is started as a reference for later rCFD predictions.

3.3. Simulation settings for rCFD

Assuming that the characteristic minimum time scale of the governing flow dynamics does not change by adding a second cubic building, we define the same sampling interval for the recurrence database $\Delta t_{rec} = 0.01$ s as in our previous study (Du et al., 2020). Based on this recurrence sampling interval, the conventional LES-based CFD simulation will write cell-to-cell communication patterns together with field data on vorticity fluctuations every 10th time step. Thanks to storage efficiency improvements in the code (not detailed in this paper), we are able to store $N = 200$ data frames. Thus, after a total simulation time of $\tau_{rec} = 2$ s, the conventional LES-based CFD simulation has established the recurrence database.

In case of island-based rCFD, we now proceed with the process of

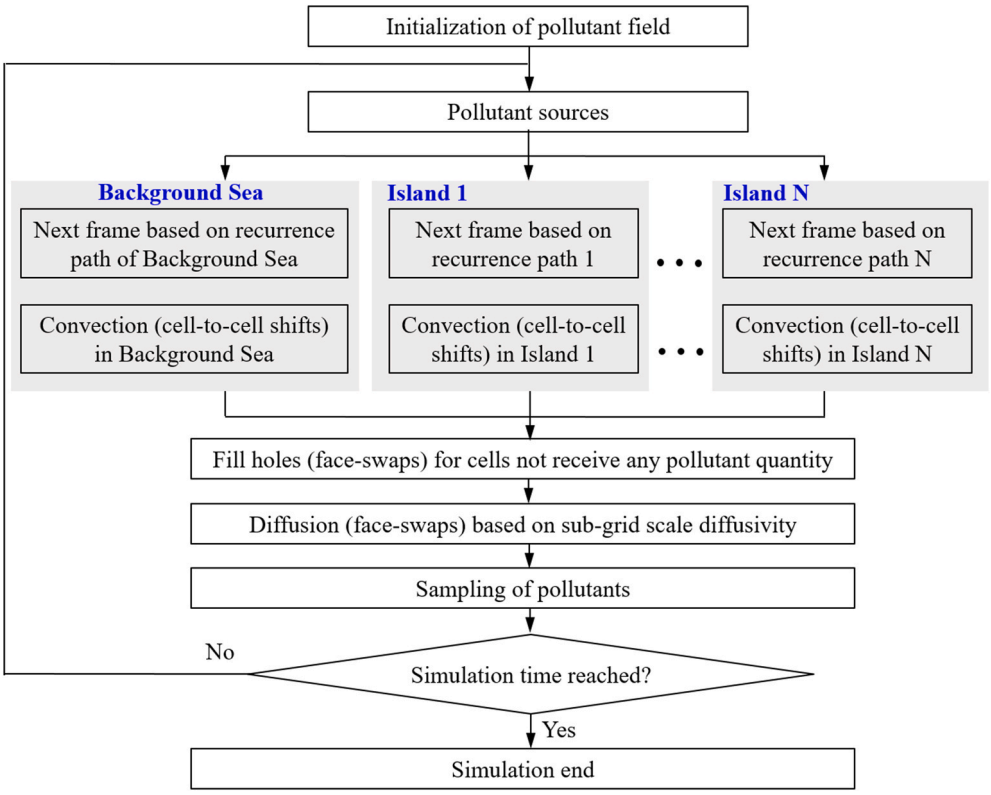

Fig. 3. Flow sheet of island-based rCFD simulations.

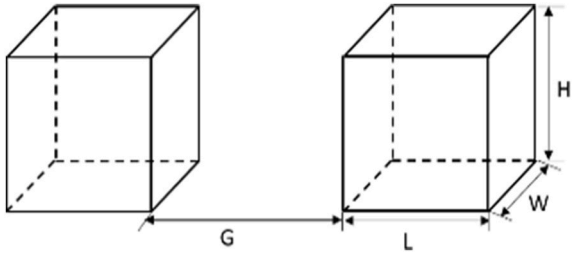

Fig. 4. Sketch of the side-by-side cubic building configurations; L = W = H = 0.05 m and G = 0.05/0.15/0.25 m.

island identification. In Fig. 6, the result of this island identification procedure can be seen. In the first small-gap configuration (Gap-1 case), only one island is identified covering both buildings. This island is embedded into a global 'background sea' of low recurrence prominence. While within this recurrence island (i.e. in the interacting wakes of those two buildings) dominant fluctuations of vorticity occur, the fluctuations of vorticity are relatively low elsewhere (i.e. in the 'background sea', which represents the rest of the domain). In case of the other two larger-gap configurations, this island topology changes such that two individual per-building islands are established. In these cases, the high fluctuation regions (i.e. in the wakes of the two buildings) are separated by an in-between region of low fluctuations, which is part of the 'background sea'. Obviously, this island formation depends on a threshold value of vorticity fluctuations magnitude which decides the formation and

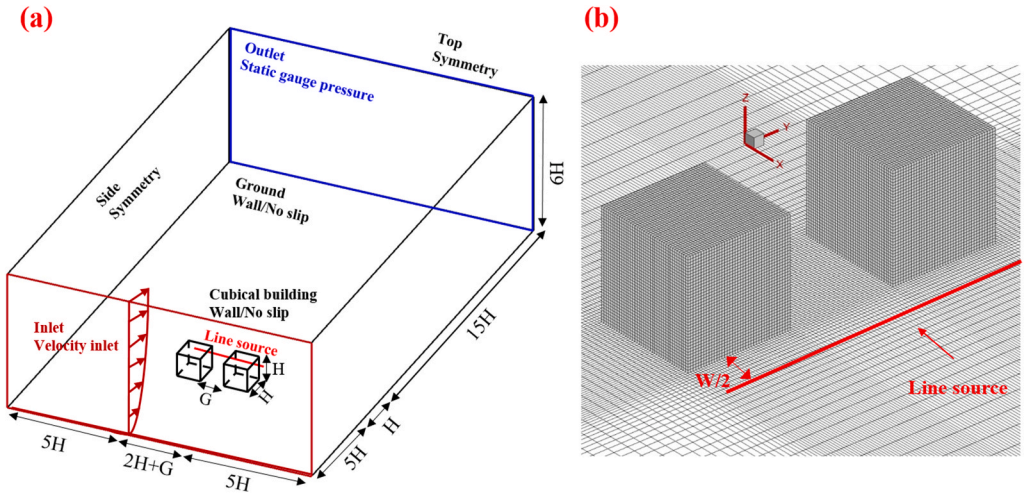

Fig. 5. (a). Computational domain for two side-by-side cubical buildings and boundary conditions; (b) cell information and line source for Gap-1 case.

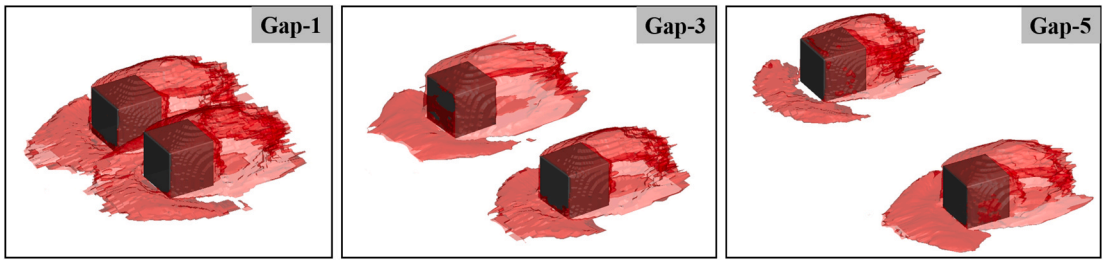

Fig. 6. Transparent iso-surfaces of island indices larger than zero indicating the position of the recurrence islands for three configurations of the two side-by-side cubical buildings; note that those islands are surrounded by a background sea with index zero.

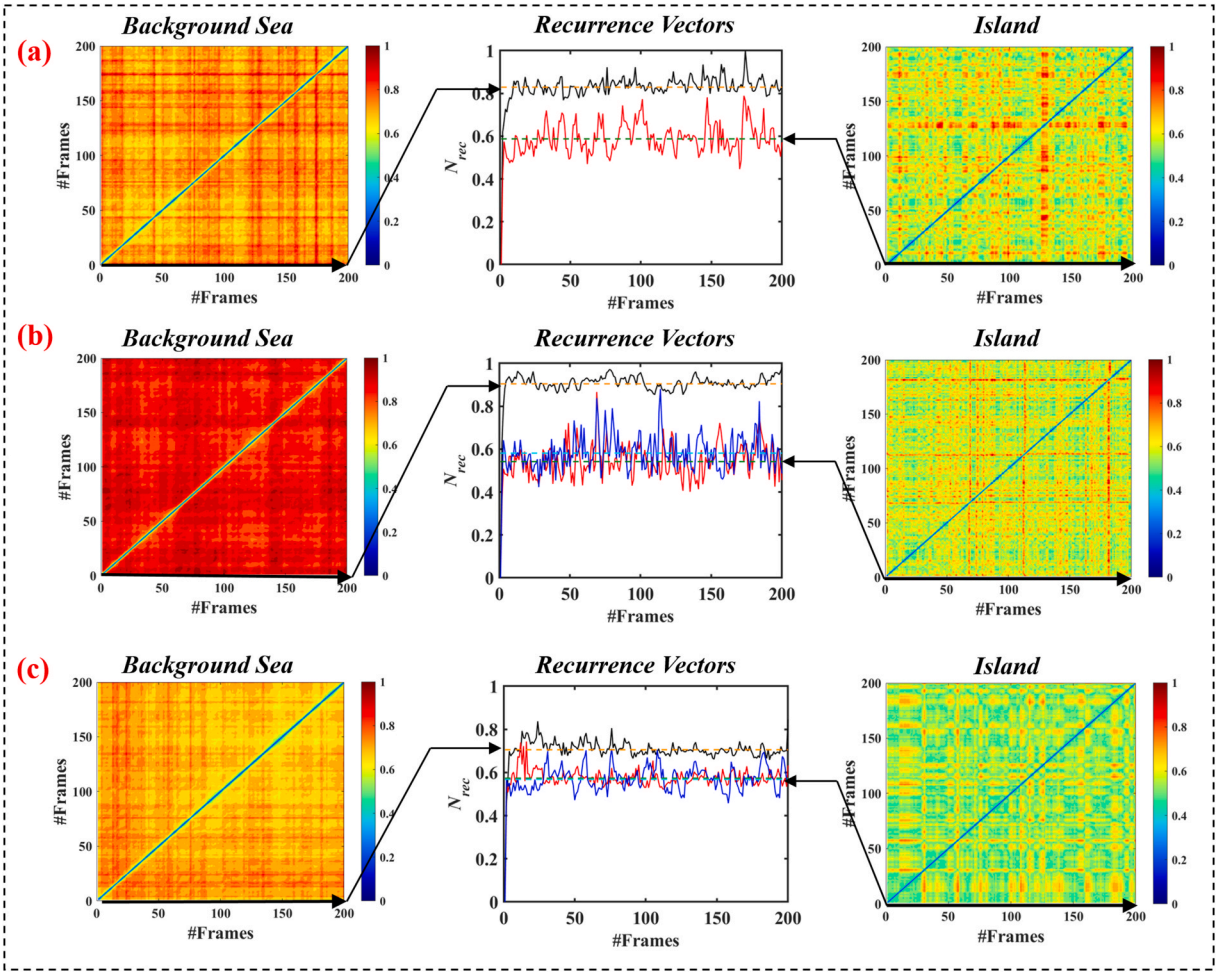

Fig. 7. Recurrence matrix and recurrence vector plots for (a) Gap-1 case, (b) Gap-3 case, and (c) Gap-5 case.

spatial extension of these recurrence islands. In order to avoid case-specific settings, we opted for a relative threshold of 15 percent of the global maximal value.

Once the domain decomposition has been established, we can separate the global database into a set of per-island databases and perform recurrence analysis on each of them. In Fig. 7, the recurrence matrices of the 'background sea' are plotted together with the recurrence matrix of the individual islands. Note that two recurrence islands have been identified for the Gap-3 and the Gap-5 cases. However, in Fig. 7 only one island's recurrence matrix is depicted, since the recurrence matrixes for these two islands are very similar. Obviously, the recurrence plateau (i.e. the mean off-diagonal level of the pairwise recurrence norms) for the island-based recurrence matrix is lower than that for the 'background sea'. Illustrating the off-diagonal behaviour of the pairwise recurrence norms along the baseline recurrence vector, we further see that within the islands we can expect a significantly higher recurrence prominence than elsewhere. Based on this per-island recurrence behaviour, different recurrence paths will be created in each individual recurrence island. In other words, we will stitch together sequences of cell-to-cell communication patterns differently for each recurrence island.

3.4. Results of CFD and rCFD simulations

In analyzing the predictive capability of rCFD, we restrict ourselves to an evaluation of mean concentration fields. For this purpose, a non-dimensional concentration coefficient (K_c) is defined as

$$K_c = \frac{cu_H H}{Q/L} \tag{8}$$

with c being the dimensional (simulated) concentration, u_H depicting the approach wind speed at building height H, Q the total pollutant emission rate and L the length of the line source.

In presenting our results, we follow a top-down approach starting with a three-dimensional iso-surface representation of the concentration plume, towards a contour plot in a horizontal plan to finally concentration profiles along vertical lines with associated error norms.

In Fig. 8 iso-surfaces of Kc are depicted illustrating the three-dimensional shape of the pollution plumes. In all cases, we can observe an accumulation of concentration in the wakes of the buildings, while the pollutants are blown downstream along the gap in between the buildings. Both versions of rCFD predict nearly the same global plume shape as the reference LES-based CFD simulation, with only minor differences in the downstream length of the pollution streaks. At this global level of evaluation, the most obvious difference can be detected in the smoothness of the iso-surfaces. While conventional LES-based CFD simulations result in very smooth mean concentration fields, both versions of rCFD introduce artificial noise into these fields, which subsequently results in an increased roughness of those iso-surfaces. This artificial noise can be linked to the representation of the continuous fluxes of pollutants by discrete cell-to-cell shifts.

In a next level of evaluation, we consider a contour plot of mean concentration in a horizontal plane at mid building height z/H = 0.5 (see Fig. 9). While both versions of rCFD successfully reproduce the main features of the reference solution, we can detect specific prediction errors in case of the global-domain based rCFD. In the Gap-3 case, the middle downstream streak is significantly over-predicted, while in case of the Gap-5 case, the two middle streaks are both underpredicted and strongly asymmetric. In this evaluation, the island-based version of rCFD achieves a better agreement with the reference solution.

Finally, we consider profiles of mean concentration at three vertical lines in the wake of one of the buildings (see Fig. 10). While the island-based rCFD agrees very well with the full LES-based CFD simulation, the global-domain based rCFD (existing rCFD) exhibits significant differences. These can be linked to locally unfavorable stitching of sequences from the global database. Stitching locally non-similar frames (representing non-similar flow features) inevitably results in local dispersion errors (e.g. when locally the flow suddenly just points into another direction). The island-based rCFD, on the other hand, provides a locally reasonable stitching of sequences (at least within the islands of most prominent recurrent fluctuations), which, in the end results in a very good predictive quality of the results. In addition to the graphical representation, Appendix A provides error norms for a quantitative evaluation of the predictive quality of island-based rCFD, which confirm the superior predictive capability of island-based rCFD simulations as opposed to the existing rCFD.

At this point, we can conclude that while both versions of rCFD are

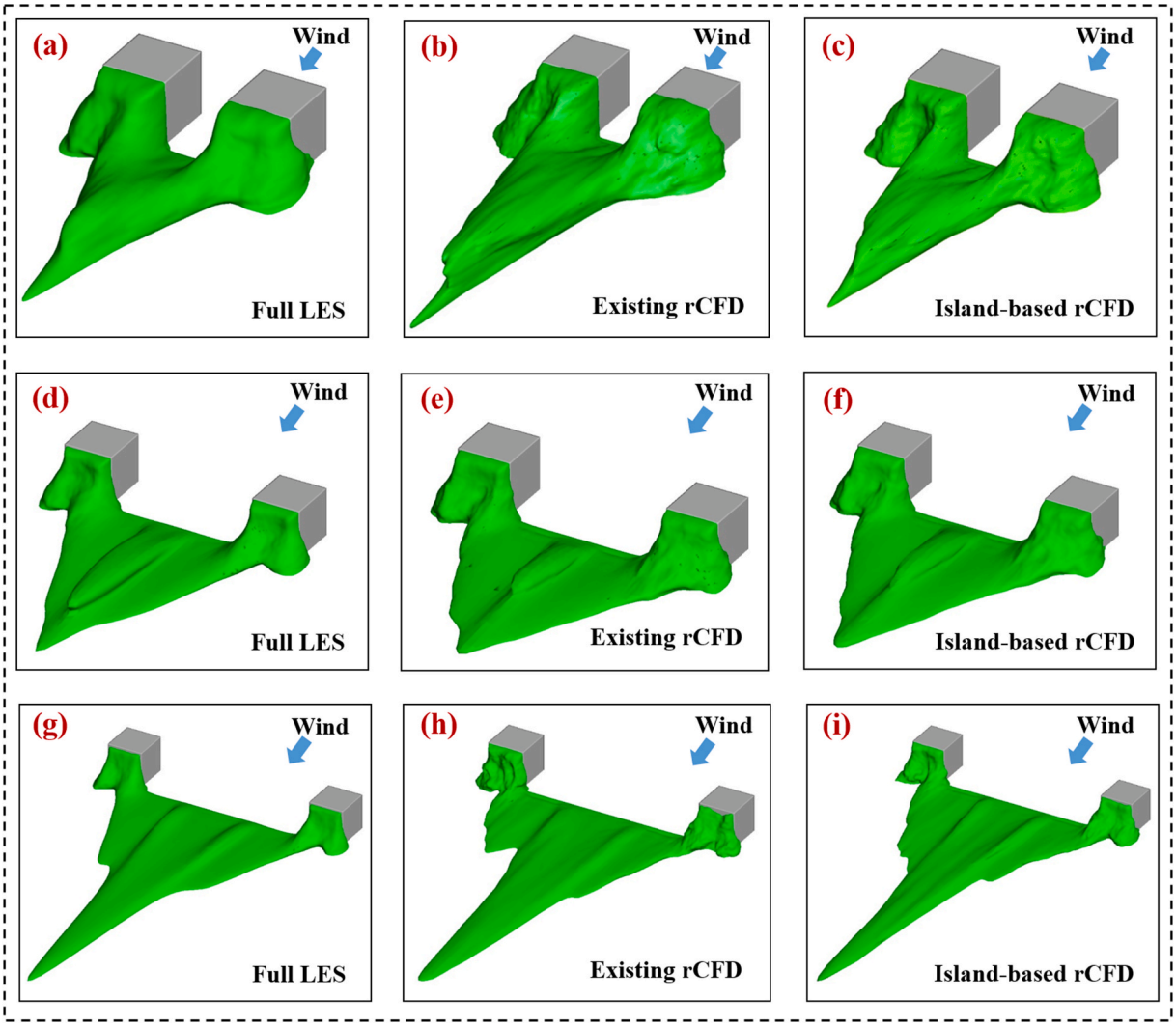

Fig. 8. Iso-surfaces of mean concentration coefficient (K_C = 3): (a–b) Gap-1 case, (c–d) Gap-3 case and (e–f) Gap-5 case.

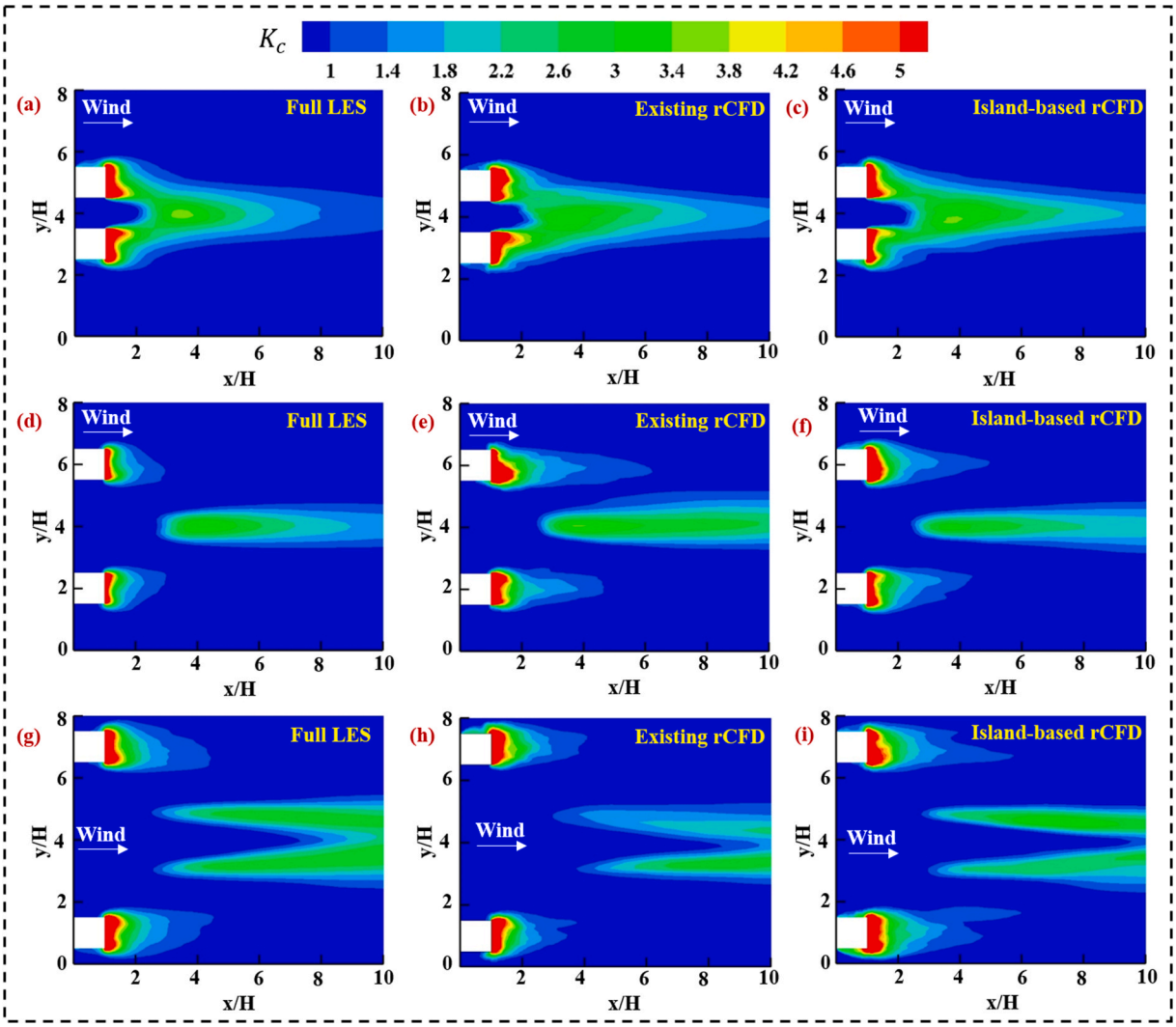

Fig. 9. Comparison of mean concentration coefficient between full LES and rCFD in horizontal plane at z/H = 0.5 for (a–c) Gap-1 case, (d–f) Gap-3 case, and (g–i) Gap-5 case.

able to picture the global behaviour of the pollutant plumes reasonably well, island-based rCFD predictions result in a better quantitative agreement with the corresponding LES-based CFD reference simulation.

At the same time, we experienced a very large speed-up in terms of computational time (see Fig. 11). While the full LES-based CFD simulations took between 300 and 400 h of wall-clock time on a 32-core computer, rCFD (both version require the same computational resources) took only 48–61 h of total simulation time, including the time needed for building the databases. This speed-up is even more pronounced, if we consider only the simulation of pollutant propagation itself, once the database has been established. In that case, rCFD simulations take just a couple of minutes (in between 11 and 14 min) in comparison to more than 300 h of corresponding full CFD simulations, resulting in a speed-up of more than three orders of magnitude (i.e. around 1500 times faster). Since the database for a given configuration has to be built up only once, this latter speed-up would represent the effective total speed-up for all subsequent simulations of alternative pollution events.

4. Application 2: A real urban environment

In the following section, we intend to prove the feasibility of island-based rCFD simulations for the prediction of pollutant dispersion in a real urban environment. In assessing the predictive capabilities and the performance of the rCFD methodology, we focus on a thorough comparison with full LES-based CFD simulations. We do not oppose our numerical predictions to measurement data, we rather restrict ourselves to a comparison between two numerical methodologies – classical LES-based CFD and island-based rCFD.

4.1. Case description

A small part of the town Linz in Austria (the home town of co-author S.P.) has been chosen as computational domain, features a dominant Wissensturm building (hosting a public library) together with some four to five storey buildings in its immediate surroundings (see Fig. 12a–b). We opted for this topology because of a planned traffic tunnel, which will have its tunnel portal located just south of this part of the town. Vehicles aiming for this tunnel might line up just in front of the Wissensturm, thus causing a dominant line-source of traffic induced pollutants. In that case, pollutant dispersion will be of crucial importance for the residents living in the wake of the Wissensturm.

4.2. Simulation settings for conventional CFD

We defined the computational domain following the same BPG as for the two side-by-side cubical building case in Section 3.2. It has dimensions $(20\,H_w + L)$ length × $(12\,H_w + W)$ width × $6\,H_w$ height. In this

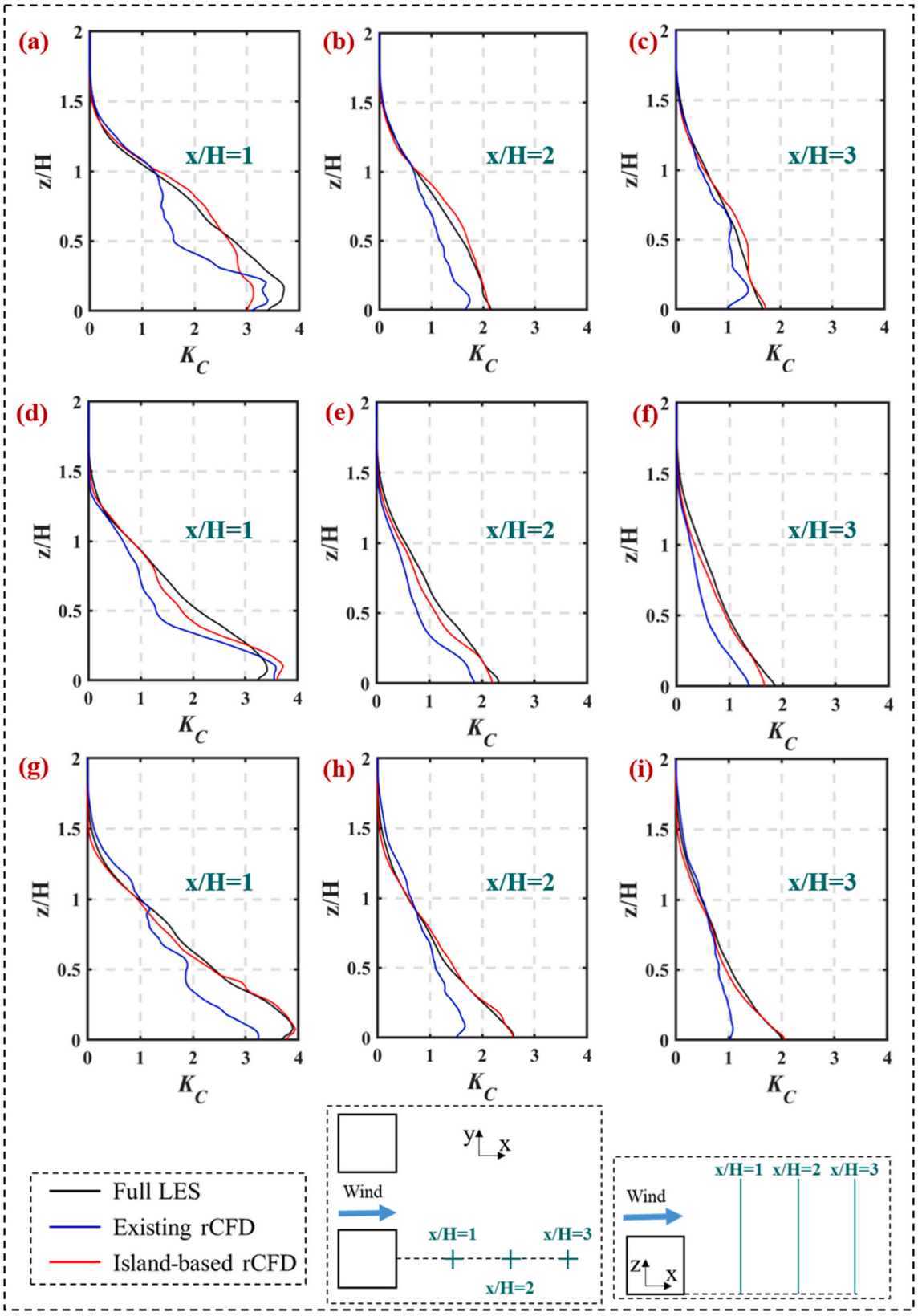

Fig. 10. Comparison of mean concentration coefficient between full LES and rCFD along 3 vertical lines downstream of one cubical building for (a–c) Gap-1 case, (d–f) Gap-3 case, and (g–i) Gap-5 case.

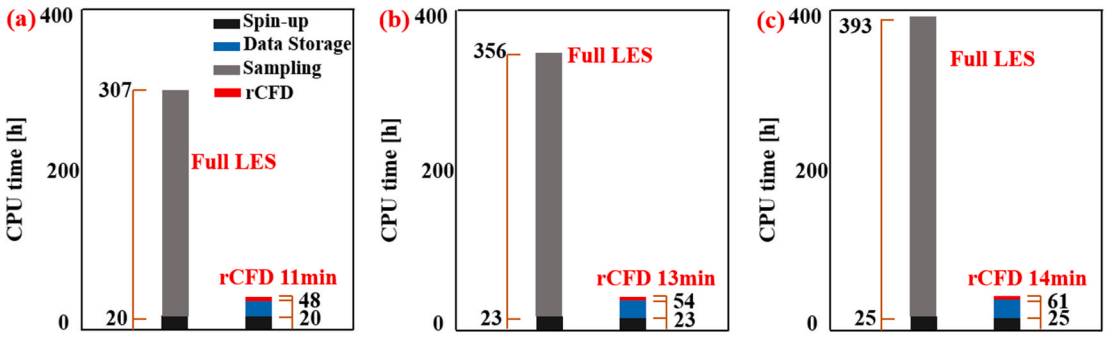

Fig. 11. CPU time consumption for three cases: (a) Gap-1 case, (b) Gap-3 case and (c) Gap-5 case.

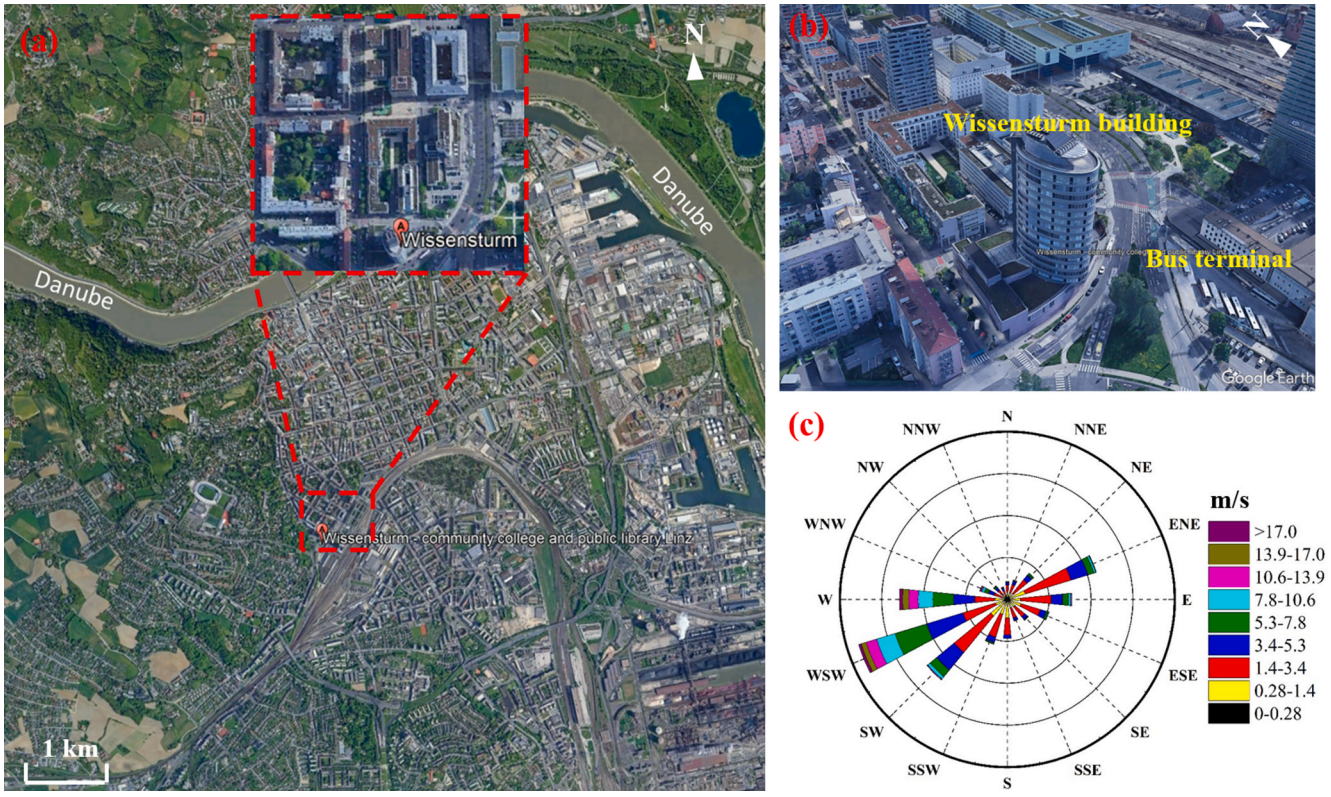

Fig. 12. Wissensturm building: (a) geographical location in Linz, Austria; (b) 3-D view of the Wissensturm building and its surrounding constructions and (c) wind rose for Linz (Climate, 2020); pictures (a,b) are generated from Google Earth.

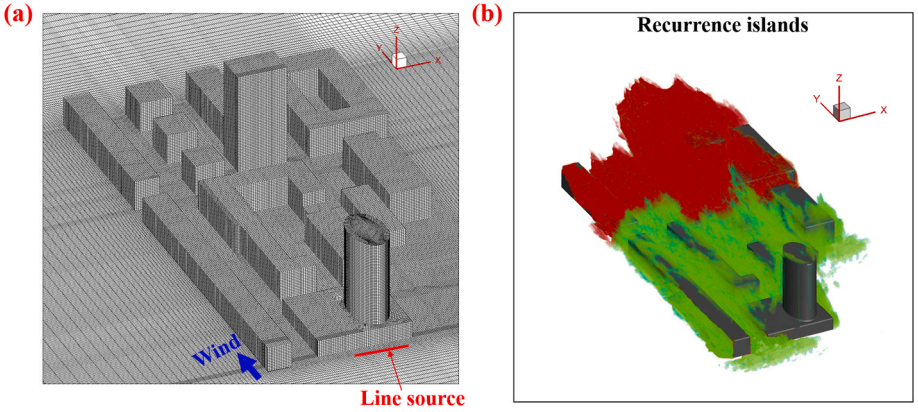

Fig. 13. (a) Grid topology together with the wind direction (blue arrow) and the position of the pollution source (red line) as well as (b) the extension of two prominent recurrence islands (red and green) covering the surroundings of the buildings.

case, $W = 200$ m and $L = 500$ m are the width and length of the building group (i.e. the chosen part of Linz) and $H_w = 63$ m is the height of the Wissensturm building. Based on this computational domain, we constructed a high-resolution computational grid with 10 million hexahedral cells by surface-grid extrusion (van Hooff and Blocken, 2010), with a minimum cell size of 1 m (see Fig. 13a).

In order to define appropriate boundary conditions, we employed a wind profile for a real urban flow in Europe from a study of Hertwig et al. (2017). More specifically, we set the vertical profiles of the incoming wind speed and turbulence intensity by interpolating the data from that study. For the reference CFD simulations, we applied the same LES (i.e. standard Smagorinsky-Lilly) modeling as described in Section 3. For the reference CFD simulation, we used time step widths of $\Delta t = 0.01$ s (with corresponding cell-based Courant numbers, $N_{Co} < 0.5$) and we controlled numerical convergence by keeping the scale residuals of all solution variables below 10^{-5}.

4.3. Simulation settings for rCFD

We determined the characteristic time step for the recurrent flow features by evaluating the average cell flow-through time (i.e. the timespan a mass-less trace would need to cross a computational cell) in interesting sub-regions within the computational domain. In our case, we opted for a recurrence time step of $\Delta t_{rec} = 1$ s, which resembles the minimum of the probed cell flow-through times. Consequently, we stored cell-to-cell communication patterns together with field data on vorticity fluctuations every 100th time-step of the LES-based reference simulation. In order to establish a database of 200 high-resolution data frames, we needed 20,000 time steps of conventional CFD.

Once the database had been established, we proceeded with the identification of recurrence islands, following the procedure illustrated in Section 2.3. In this case, this identification procedure yielded two prominent recurrence islands, which are illustrated in Fig. 13b. In contrast to the previous side-by-side building case, these islands are not separated by a background sea of low recurrence prominence (instead, these islands are surrounded by a low-prominence background sea). Nevertheless, an evaluation of the respective recurrence matrixes and recurrence vectors reveals that also in this case the recurrence prominence within the islands is significantly enhanced (see Fig. 14). While the recurrence vector of the remaining background sea shows nearly no off-diagonal features, both recurrence islands exhibit prominent off-diagonal minima (indicating similar frame pairings). Given the low recurrence prominence of the background sea, we abstain from a global-domain based rCFD simulation and in the following solely apply the island-based version of rCFD.

4.4. Results of CFD and rCFD simulations

In the case of a real urban environment with the associated large computational grids, assessing average concentration fields requires very long simulation times for the reference LES-based CFD simulation. Based on our available computational resources we estimated the necessary simulation time in the order of several months. In order to avoid such excess simulation costs, we therefore decided to focus on the time-evolving instantaneous concentration patterns during an unsteady pollution event. More specifically, we considered a line source of pollutants which is activated at some instance of time and subsequently simulate the propagation of that pollutant within an initially unpolluted environment.

In turbulent flows, any unsteady propagation depends on the specific flow realization at the very instance of time. The concentration patterns of two LES-based CFD simulations will differ, depending on the specific starting time of the pollution source. In order to obtain a representative unsteady propagation, one would have to apply ensemble averaging (i.e. averaging the results of many unsteady pollution events), which once again would lead to excessive computational times. In our study, we therefore compared only one unsteady reference CFD simulation to several realizations of island-based rCFD simulations (which, in turn, do not consume significant computational resources). In comparing the results, we have to keep in mind that even the best possible outcome cannot be expected to be a perfect agreement (like in Section 3), since we compare individual realizations of an unsteady propagation event in turbulent flow.

In presenting the comparative results, we employ the same top-down approach as in Section 3.4, starting with three-dimensional iso-surfaces of the concentration plumes, followed by contour plots of concentration at pedestrian level and concentration profiles along vertical lines with associated error norms.

In Fig. 15 iso-surfaces of the instantaneous concentration fields at three and six minutes after the start of the pollution source are depicted, illustrating the three-dimensional extension of the instantaneous pollution plumes.

The island-based rCFD successfully reproduces the general features of plume shape as the reference LES-based CFD simulation. On the west of the Wissensturm, the street canyon is quickly filled with pollutants, while in relation to that the atrium in the wake of the building remains nearly free of pollutants. On the east side of the Wissensturm the downstream spreading of pollutants is hindered by several lower buildings.

Beyond these main features some clear differences are observed. As expected, there are not only differences between rCFD predictions and the reference CFD simulation, but also between the two realizations of rCFD. In general, the reference simulation seems to be more dispersive than both rCFD simulations (i.e. the pollution plume of the reference simulation extends further to the right and to the left). We attribute this to flow features which are part of the long-term CFD simulation, but which are not represented in the limited database of the rCFD simulations.

Next, contour plots of concentration fields at pedestrian level (z = 2 m) are given in Fig. 16. Instead of plotting instantaneous values of concentration, we here present a time-averaged concentration field, with time-averaging applied from the start until 6 min after the

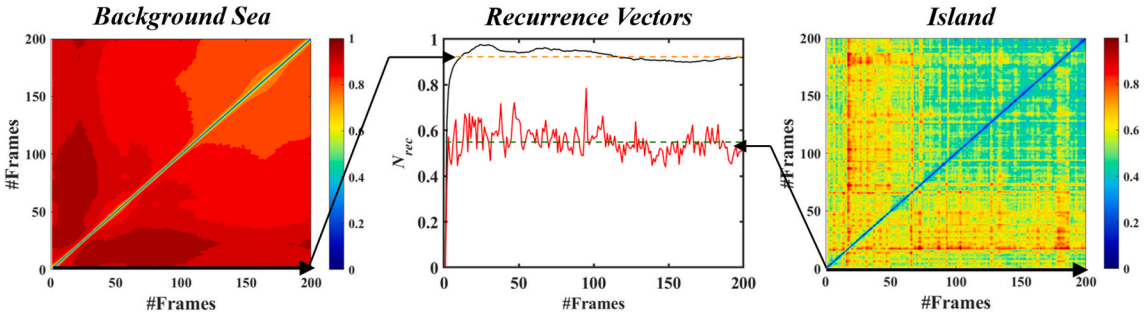

Fig. 14. Recurrence matrix and recurrence vector plots for the real urban environment case for the background sea (left) and one recurrence island (right); note that only one recurrence island is considered for the sake of simplicity.

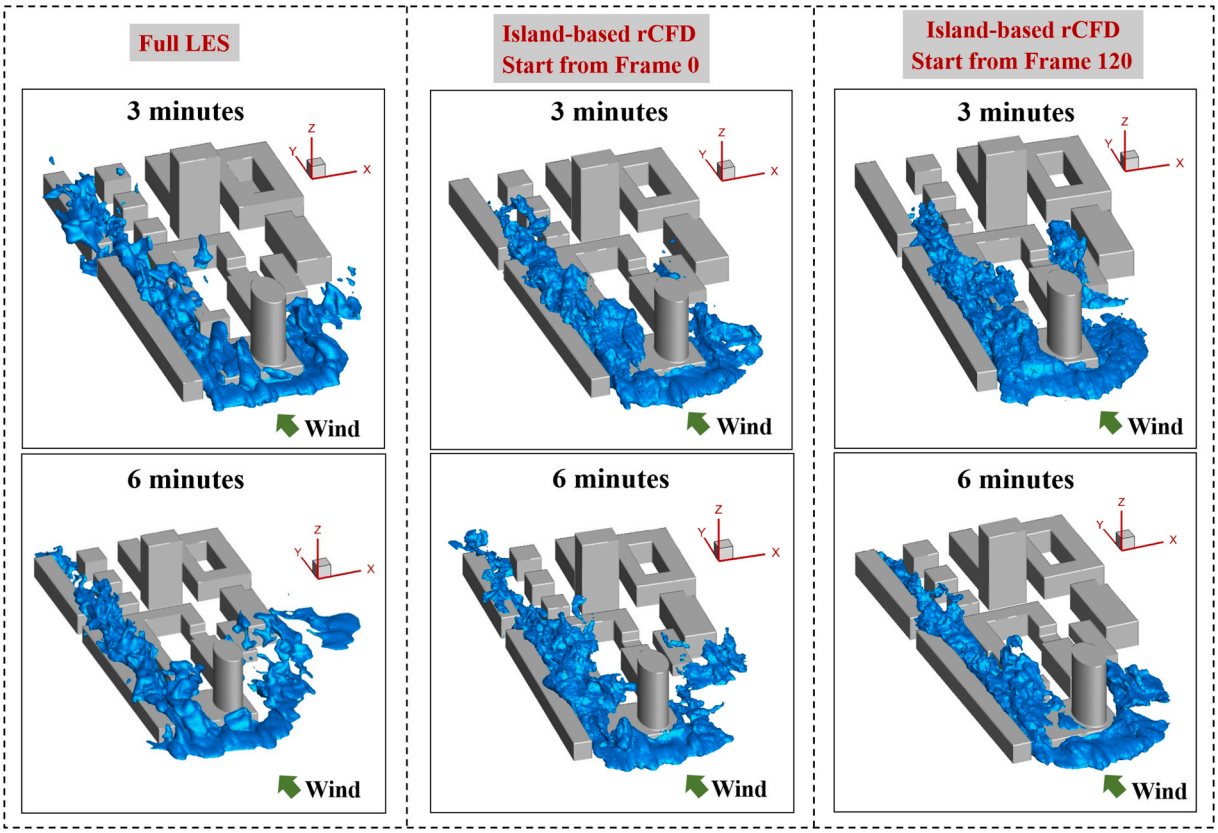

Fig. 15. Iso-surfaces of instantaneous concentration (K_C = 0.18) three (top row) and six (bottom row) minutes after activation of the pollution source; full CFD simulations (left) are opposed to two realizations of island-based rCFD (middle and right).

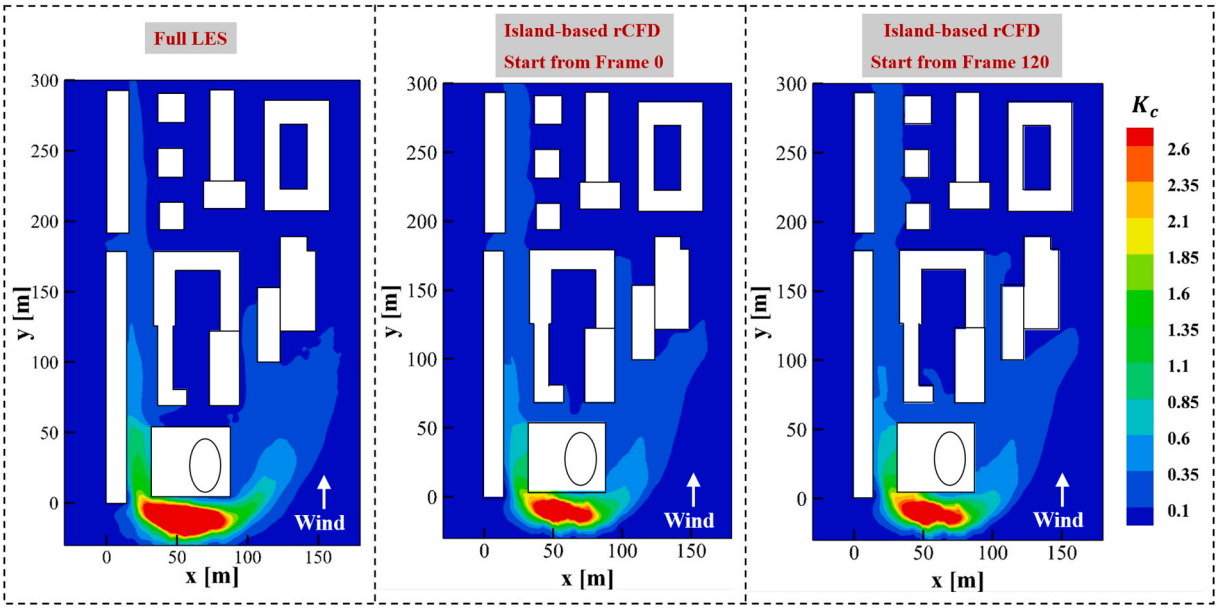

Fig. 16. Time-averaged concentration fields at pedestrian level (z = 2 m) 6 min after activating the pollution source; reference LES-based CFD (left) and two realizations of island-based rCFD (middle, right).

activation of the pollution source. This comparison shows a generally good agreement between the reference CFD simulations and the two realizations of rCFD, especially in the wake of the Wissensturm. However, just up-stream of the Wissensturm, the reference CFD simulation predicts a more pronounced local accumulation of pollutants than both rCFD simulations. This discrepancy might be linked to the fact that the line source has been placed into an upstream recirculation zone, which is prone to discretization errors by mass-less tracers (which we need to evaluate cell-to-cell connectivity).

In Fig. 17 concentration profiles are given along five vertical lines. Also in this case, we applied 6 min of time-averaging in order to obtain time-marching mean values of concentration. While we still see a

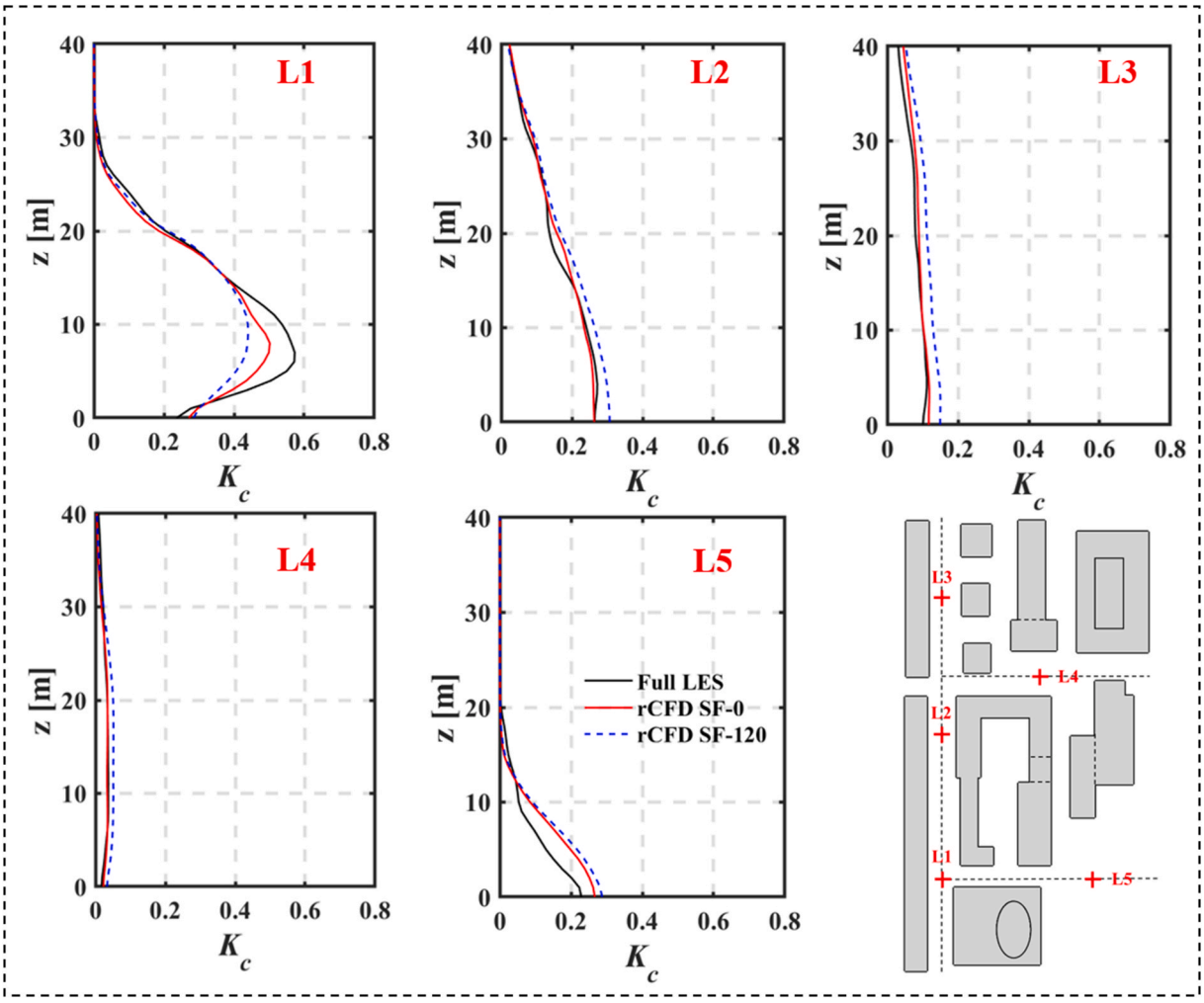

Fig. 17. Time-averaged pollution concentration profiles at five vertical lines, comparing the reference CFD simulation with two realizations of rCFD simulations; in the right insert the position of the profiles is given.

generally good agreement between the reference CFD simulation and the two realizations of rCFD, we can observe significant differences especially at the line L1 and L5. Those profiles are most affected by the local accumulation of pollutants upstream of the Wissensturm, which is under-predicted by both rCFD simulations. A quantitative evaluation of these profiles based on available error norms is given in Appendix A.

For the case of a real urban environment, we experienced an even larger computational speed-up than in the case of the side-by-side buildings. While the LES-based reference simulation took 320 h of wall-clock time on a 32-core computer in order to cover 6 min of pollution dispersion, each rCFD simulation required only 3.7 min (on the same hardware) yielding a relative speed-up of more than five thousand (i.e. rCFD simulations run 5.189 times faster than conventional LES-based CFD simulations). Notably, this speed-up leads to faster-than-real-time simulation of pollutant dispersion at high resolution (i.e. on a computation grid of 10 million cells).

5. Conclusion

In this study, we performed recurrence CFD (rCFD) simulations of near-field pollutant dispersion in two topologies. In order to overcome the insufficient recurrence prominence of the global flow field, we developed a new methodology to decompose the computational domain into distinct islands of high recurrence prominence. Subsequently, we tested the novel island-based rCFD by two application examples, namely (i) a two side-by-side cubical buildings configuration and (ii) a real urban environment.

The main findings for the two side-by-side building case are as follows:

i) Predictions of island-based rCFD agree well with corresponding results of a full LES-based reference CFD simulation in terms of three-dimensional iso-surfaces of the concentration plume, contour plots in a horizontal plane and concentration profiles along vertical lines.
ii) Compared to existing global-domain rCFD simulations, the novel island-based rCFD simulations have an improved predictive capability, yielding excellent agreement with the LES-based reference CFD simulation.
iii) Island-based rCFD simulations are about a thousand times faster than corresponding LES-based CFD simulations.

The main findings for the real urban environment case are as follows:

iv) Island-based rCFD simulations of pollutant dispersion on a large computational grid of 10 million cells are feasible and deliver reasonable results.
v) Qualitatively, predictions of island-based rCFD agree fairly well with corresponding results by a LES-based reference CFD simulation in terms of three-dimensional iso-surface of the instantaneous concentration plume, contour plots in a horizontal plane and concentration profiles along vertical lines.

vi) Existing quantitative discrepancies between island-based rCFD predictions and the reference LES-based CFD simulation can be linked to an obvious under-prediction of local pollution accumulation in the upstream recirculation bubble in front of the Wissensturm.
vii) Island-based rCFD simulations are about five-thousand times faster than corresponding LES-based CFD simulations yielding faster-than-real-time simulations of pollutant dispersion at high resolution.

Overall, this study demonstrates that near-field pollutant dispersion within complex urban environment can be efficiently modelled by island-based rCFD.

Software availability

Software name: ANSYS FLUENT;
Contact address: South-pointe, 2600 ANSYS Drive, Canonsburg, PA 15317, USA;
Program language: C/C++
Software Availability: The software could be purchased for academic purposes upon request.
Website: www.ansys.com.
Recurrence CFD implementation: User Defined Functions in ANSYS FLUENT.
Program language: C/C++

Declaration of competing interest

The authors declare that they have no known competing financial interests or personal relationships that could have appeared to influence the work reported in this paper.

Acknowledgement

The authors acknowledge the financial contribution of the Linz Institute of Technology (LIT-2017-3-SEE-008 and LIT-2016-1-YOU-007).

Appendix A. Error norms

In order to quantify discrepancies along concentration profiles, we employ four common error norms – linear correlation coefficient (R), fraction of predictions within a factor of two of observations (FAC2), fractional bias (FB), and normalized mean square error (NMSE). These error norms are given by,

$$R = \frac{\frac{1}{n}\sum_i (K_{rCFD} - K_{rCFD})(K_{LES} - K_{LES})}{\sigma_{K_{rCFD}} \sigma_{K_{LES}}} \tag{A.1}$$

$$FAC2 = \frac{1}{n}\sum_i F_i \; F_i = \begin{cases} 1, \; if \; 0.5 \le \dfrac{K_{rCFD}}{K_{LES}} \le 2 \\ 0, \; else \end{cases} \tag{A.2}$$

$$FB = \frac{\sum_i (K_{rCFD} - K_{LES})}{0.5\sum_i (K_{rCFD} + K_{LES})} \tag{A.3}$$

$$NMSE = \frac{1}{n}\sum_i (K_{rCFD} - K_{LES})^2 \Big/ (K_{rCFD} K_{LES}) \tag{A.4}$$

In case of perfect agreement, these error norms would account to $R = 1$, FAC2 = 1, $FB = 0$ and $NMSE = 0$, respectively. According to the suggestions from literatures (Hanna et al., 2004; Tominaga and Stathopoulos, 2018), the numerical predictions are considered as being sufficiently good for $R >$ 0.8, FAC2 > 0.5, |FB| < 0.3, and NMSE <0.4.

For the case of the two side-by-side buildings the error norms applied for the three vertical lines in Fig. 10 are summarized in Table 1.

Table 1
Error norms for concentration profiles; side-by-side buildings

Lines	R	FAC2	FB	NMSE
Gap-1				
x/H = 1	0.985	0.895	−0.051	0.387
x/H = 2	0.995	0.900	0.047	0.123
x/H = 3	0.996	0.911	0.049	0.119
Gap-3				
x/H = 1	0.985	0.891	−0.042	0.361
x/H = 2	0.996	0.899	−0.071	0.225
x/H = 3	0.998	0.919	−0.078	0.149
Gap-5				
x/H = 1	0.998	0.959	−0.015	0.227
x/H = 2	0.999	0.968	0.022	0.124
x/H = 3	0.998	0.977	−0.034	0.104

For all profiles the R values are larger than 0.98, indicating a very strong linear relationship between island-based rCFD and the reference simulation. All the values of FAC2 are above 0.89, especially for the Gap-5 case (above 0.95), suggesting the results by island-based rCFD agrees well with full LES in general. Similarly, all absolute FB values are very small and all NMSE values are well below 0.4, which means that both the systematic and random errors are very low. Based on these error norms, we can conclude that island-based rCFD simulations can produce very similar pollutant

results as full LES.

For the case of real urban environment, the error norms applied for the three vertical lines in Fig. 17 are summarized in Table 2. While most of these error norms still meet the above stated recommendations from literature (Hanna et al., 2004; Tominaga and Stathopoulos, 2018), we have to accept significantly larger errors than in the previous case. Especially, for concentration profiles close to the upstream recirculation area (i.e. L1 and L5) we for instance get rather low values for the FAC2 error norm.

Table 2
Error norms for concentration profiles; real urban environment

Lines	*R*	FAC2	FB	NMSE
L1	0.995	0.800	−0.097	0.112
L2	0.996	1.000	−0.013	0.004
L3	0.993	1.000	0.109	0.011
L4	0.978	0.900	−0.056	0.028
L5	0.987	0.601	0.260	0.958

References

Abbasi, S., Pirker, S., Lichtenegger, T., 2020. Application of recurrence CFD (rCFD) to species transport in turbulent vortex shedding. Comput. Fluids 196, 104348.

Ai, Z., Mak, C.M., 2014. Modeling of coupled urban wind flow and indoor air flow on a high-density near-wall mesh: sensitivity analyses and case study for single-sided ventilation. Environ. Model. Software 60, 57–68.

ANSYS Fluent 19.0. Theory Guide, 2018. ANSYS Inc.

Bartzis, J.G., Sfetsos, A., Andronopoulos, S., 2008. On the individual exposure from airborne hazardous releases: the effect of atmospheric turbulence. J. Hazard Mater. 150 (1), 76–82.

Block, M.L., Calderón-Garcidueñas, L., 2009. Air pollution: mechanisms of neuroinflammation and CNS disease. Trends Neurosci. 32 (9), 506–516.

Blocken, B., 2014. 50 years of computational wind engineering: past, present and future. J. Wind Eng. Ind. Aerod. 129, 69–102.

Blocken, B., 2018. LES over RANS in building simulation for outdoor and indoor applications: a foregone conclusion? Build Simul. 821–870.

Blocken, B., Gualtieri, C., 2012. Ten iterative steps for model development and evaluation applied to computational fluid dynamics for environmental fluid mechanics. Environ. Model. Software 33, 1–22.

Blocken, B., Janssen, W., van Hooff, T., 2012. CFD simulation for pedestrian wind comfort and wind safety in urban areas: general decision framework and case study for the Eindhoven University campus. Environ. Model. Software 30, 15–34.

Blocken, B., Tominaga, Y., Stathopoulos, T., 2013. CFD simulation of micro-scale pollutant dispersion in the built environment. Build. Environ. 64, 225–230.

Chu, A., Kwok, R.C.-W., Yu, K., 2005. Study of pollution dispersion in urban areas using computational fluid dynamics (CFD) and geographic information system (GIS). Environ. Model. Software 20 (3), 273–277.

Climate Linz. https://www.meteoblue.com/en/weather/historyclimate/climatemodelled/linz_austria_2772400. (Accessed 31 August 2020).

Cui, D., Mak, C.M., Ai, Z., Kwok, K.C., Meng, X., Niu, J., 2017. On-site evaluation of pedestrian-level air quality at a U-type street canyon in an ancient city. J. Wind Eng. Ind. Aerod. 168, 322–333.

Dabbagh, F., Pirker, S., Schneiderbauer, S., 2020. On the fast modeling of species transport in fluidized beds using recurrence computational fluid dynamics. AIChE J. 66 (5), 16931.

Du, Y., Mak, C.M., Ai, Z., 2018. Modelling of pedestrian level wind environment on a high-quality mesh: a case study for the HKPolyU campus. Environ. Model. Software 103, 105–119.

Du, Y., Blocken, B., Pirker, S., 2020. A novel approach to simulate pollutant dispersion in the built environment: transport-based recurrence CFD. Build. Environ. 170, 106604.

Environmental Protection Agency. Air quality - national summary. https://www.epa.gov/air-trends/air-quality-national-summary. (Accessed 26 August 2020).

Giles-Corti, B., Vernez-Moudon, A., Reis, R., Turrell, G., Dannenberg, A.L., Badland, H., Foster, S., Lowe, M., Sallis, J.F., Stevenson, M., 2016. City planning and population health: a global challenge. Lancet 388, 2912–2924.

Gousseau, P., Blocken, B., van Heijst, G.J., 2012. Large-Eddy Simulation of pollutant dispersion around a cubical building: analysis of the turbulent mass transport mechanism by unsteady concentration and velocity statistics. Environ. Pollut. 167, 47–57.

Gromke, C., Ruck, B., 2012. Pollutant concentrations in street canyons of different aspect ratio with avenues of trees for various wind directions. Bound.-Layer Meteorol 144 (1), 41–64.

Gromke, C., Jamarkattel, N., Ruck, B., 2016. Influence of roadside hedgerows on air quality in urban street canyons. Atmos. Environ. 139, 75–86.

Hanna, S.R., Hansen, O.R., Dharmavaram, S., 2004. FLACS CFD air quality model performance evaluation with Kit Fox, MUST, Prairie Grass, and EMU observations. Atmos. Environ. 38 (28), 4675–4687.

Hertwig, D., Patnaik, G., Leitl, B., 2017. LES validation of urban flow, part I: flow statistics and frequency distributions. Environ. Fluid Mech. 17 (3), 521–550.

Li, W.-W., Meroney, R.N., 1983. Gas dispersion near a cubical model building. Part I. Mean concentration measurements. J. Wind Eng. Ind. Aerod. 12 (1), 15–33, 1983.

Lichtenegger, T., 2018. Local and global recurrences in dynamic gas-solid flows. Int. J. Multiphas. Flow 106, 125–137.

Lichtenegger, T., Pirker, S., 2016. Recurrence CFD – a novel approach to simulate multiphase flows with strongly separated time scales. Chem. Eng. Sci. 153, 394–410.

Lilly, K., 1966. On the Application of the Eddy Viscosity Concept in the Inertial Sub-range of Turbulence. National Center for Atmospheric Research, Boulder, CO. NCAR Manuscript No. 123.

Moonen, P., Allegrini, J., 2015. Employing statistical model emulation as a surrogate for CFD. Environ. Model. Software 72, 77–91.

Moonen, P., Dorer, V., Carmeliet, J., 2011. Evaluation of the ventilation potential of courtyards and urban street canyons using RANS and LES. J. Wind Eng. Ind. Aerod. 99 (4), 414–423.

Niu, J., Tung, T., 2007. On-site quantification of re-entry ratio of ventilation exhausts in multi-family residential buildings and implications. Indoor Air 18 (1), 12–26.

Pirker, S., Lichtenegger, T., 2018. Efficient time-extrapolation of single- and multiphase simulations by transport based recurrence CFD (rCFD). Chem. Eng. Sci. 188, 65–83.

Pirker, S., Puttinger, S., Rössler, R., Lichtenegger, T., 2020. Steel Alloy Homogenization during Rheinsahl–Heraeus Vacuum Treatment: Conventional Computational Fluid Dynamics, Recurrence Computational Fluid Dynamics, and Plant Observations. Steel Research International, pp. 12–13.

Pope, S.B., 2000. Turbulent Flows. Cambridge University Press, Cambridge.

Rajaona, H., Septier, F., Armand, P., Delignon, Y., Olry, C., Albergel, A., Moussafir, J., 2015. An adaptive Bayesian inference algorithm to estimate the parameters of a hazardous atmospheric release. Atmos. Environ. 122, 748–762.

Ricci, A., Burlando, M., Repetto, M.P., Blocken, B., 2019. Simulation of urban boundary and canopy layer flows in port areas induced by different marine boundary layer inflow conditions. Sci. Total Environ. 670, 876–892.

Schatzmann, M., Olesen, H., Franke, J., 2010. COST 732 Model Evaluation Case Studies: Approach and Results. COST Office, Brussels, Belgium.

Senocak, I., Hengartner, N.W., Short, M.B., Daniel, W.B., 2008. Stochastic event reconstruction of atmospheric contaminant dispersion using Bayesian inference. Atmos. Environ. 42 (33), 7718–7727, 2008.

Shorshani, M.F., André, M., Bonhomme, C., Seigneur, C., 2015. Modelling chain for the effect of road traffic on air and water quality: techniques, current status and future prospects. Environ. Model. Software 64, 102–123.

Smagorinsky, J., 1963. General circulation experiments with the primitive equations: I. The basic experiment. Mon. Weather Rev. 91 (3), 99–164.

Tominaga, Y., Stathopoulos, T., 2013. CFD simulation of near-field pollutant dispersion in the urban environment: a review of current modeling techniques. Atmos. Environ. 79, 716–730.

Tominaga, Y., Stathopoulos, T., 2018. CFD simulations of near-field pollutant dispersion with different plume buoyancies. Build. Environ. 131, 128–139.

Tominaga, Y., Mochida, A., Yoshie, R., Kataoka, H., Nozu, T., Yoshikawa, M., Shirasawa, T., 2008. AIJ guidelines for practical applications of CFD to pedestrian wind environment around buildings. J. Wind Eng. Ind. Aerod. 96 (10–11), 1749–1761.

van Hooff, T., Blocken, B., 2010. Coupled urban wind flow and indoor natural ventilation modelling on a high-resolution grid: a case study for the Amsterdam ArenA stadium. Environ. Model. Software 25 (1), 51–65.

Zhong, J., Cai, X.M., Bloss, W.J., 2016. Coupling dynamics and chemistry in the air pollution modelling of street canyons: a review. Environ. Pollut. 214, 690–704.